[5] M. Swaminathan, E. Arvas, T. K. Sarkar, and A. R. Djordjevic, "Computation of cutoff wavenumbers of TE and TE Modes in waveguides of arbitrary cross sections using a surface integral formulation," *IEEE Trans. Microwave Theory Tech.*, vol. 38, pp. 154–159, Feb. 1987.

[6] C. E. Baum, "Toward an engineering theory of electromagnetic scattering: the singularity and eigenmode expansion method," in *Electromagnetic Scattering*, P. L. E. Uslenghi, Ed. London: Academic Press, 1978.

An Efficient Algorithm for Transmission Line Matrix Analysis of Electromagnetic Problems Using the Symmetrical Condensed Node

Cheuk-yu Edward Tong and Yoshiyuki Fujino

Abstract—**The symmetrical condensed TLM node has been closely examined. An efficient algorithm has been developed from the results of this study which significantly improves the numerical efficiency of the node. Certain physical aspects of the symmetrical condensed node are also discussed.**

I. Introduction

The transmission line matrix (TLM) method has now been established, owing to the works of Johns [1] and Hoefer [2], as one of the most powerful time-domain solvers of electromagnetic problems [3], [4].

The symmetrical condensed node invented by Johns [5] has proved to be a particularly valuable tool in TLM analysis. Since it represents both the electric and the magnetic field at the same point in space, it is more attractive than the expanded node used in other TLM networks [6], in the Finite-Difference Time-Domain (FDTD) method [7], and in the spatial network method [8]. Besides, as a consequence of the simplicity of node topology, ambiguities of interfaces and boundaries are removed. The node has recently been extended to cover lossy media [9].

The disadvantage of the symmetrical condensed node is that no equivalent circuit can be drawn up to represent it. It is solely characterized by a scattering matrix. The user, therefore, has to perform a linear transformation using an 18×18 scattering matrix at each nodal point. This means that the numerical efficiency is inherently low. Further, the nature of this scattering matrix has rarely been discussed.

In this paper, we demonstrate that an efficient algorithm can be obtained for the symmetrical condensed node. Such an algorithm not only shortens the computation time but also helps to unlock the physics hidden behind the scattering matrix. We shall first discuss the case of the original node before moving on to the lossy node. Finally, numerical examples will be presented.

Manuscript received October 11, 1990; revised April 29, 1991.

C. E. Tong was the Communications Research Laboratory, Tokyo, Japan. He is now with the Harvard-Smithsonian Center for Astrophysics, 60 Garden St., Cambridge, MA 02138.

Y. Fujino is with the Communications Research Laboratory, 4-2-1 Nukui-Kitamachi, Koganei-shi, Tokyo, 184 Japan.

IEEE Log Number 9101373.

II. The Symmetrical Condensed Node

The basic structure of the symmetrical condensed node as proposed by Johns is given in Fig. 1. It is connected to each of its six neighbors by a pair of transmission lines, carrying orthogonal polarizations. These lines are numbered 1 to 12. The node is also connected to six stubs, one for each field component. The three electric or permittivity stubs (numbered 13 to 15) are open-circuit, while the magnetic or permeability stubs (16 to 18) are short-circuit. Hence, each node receives 18 input impulses at each time step.

Scattering takes place at the center of the node. The 18 input impulses $\underline{V}^i$ are scattered to produce 18 output impulses $\underline{V}^s$ into the 18 ports:

$$\underline{V}^s = \boldsymbol{S}\cdot\underline{V}^i. \tag{1}$$

The scattering matrix, $\boldsymbol{S}$, has been derived by Johns from Maxwell's equations and is shown in Fig. 2. The elements of the matrix assume the following values:

$$a_{pq} = \frac{-Y_p}{2(4+Y_p)} + \frac{Z_q}{2(4+Z_q)}$$

$$b_p = e_p = \frac{4}{2(4+Y_p)}$$

$$c_{pq} = \frac{-Y_p}{2(4+Y_p)} - \frac{Z_q}{2(4+Z_q)}$$

$$d_q = i_q = \frac{4}{2(4+Z_q)}$$

$$f_q = Z_q d_q$$

$$g_p = Y_p b_p$$

$$h_p = \frac{(Y_p-4)}{(Y_p+4)}$$

$$j_q = \frac{(4-Z_q)}{(4+Z_q)}$$

where the subscripts $p, q = x$, y, or z. The subscript p is related to the associated permittivity stub of the port in question and q is related to the associated permeability stub (See Fig. 2 for the associations). For example,

$$S_{29} = c_{xy}.$$

Note that Y_p is the normalized characteristic admittance of the electric stub p, and Z_q is the normalized characteristic impedance of the magnetic stub q.

III. The Scattering Matrix

Although the scattering matrix appears to be very complicated, it possesses a high degree of symmetry. We have ex-

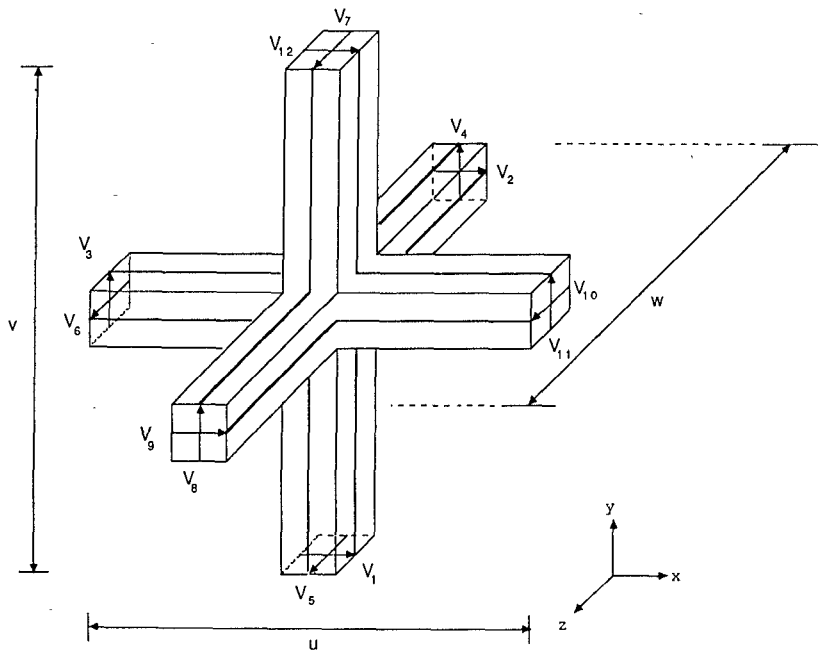

Fig. 1. The symmetrical condensed TLM node.

ploited this symmetry to derive the following expressions:

$$U_x = (V_1^s + V_{12}^s) + (V_2^s + V_9^s) + Y_x V_{13}^s = (V_1^i + V_{12}^i) + (V_2^i + V_9^i) + Y_x V_{13}^i \quad (2)$$

$$U_y = (V_3^s + V_{11}^s) + (V_4^s + V_8^s) + Y_y V_{14}^s = (V_3^i + V_{11}^i) + (V_4^i + V_8^i) + Y_y V_{14}^i \quad (3)$$

$$U_z = (V_5^s + V_7^s) + (V_6^s + V_{10}^s) + Y_z V_{15}^s = (V_5^i + V_7^i) + (V_6^i + V_{10}^i) + Y_z V_{15}^i \quad (4)$$

$$J_x = (V_4^s - V_8^s) - (V_5^s - V_7^s) - V_{16}^s = -\left[(V_4^i - V_8^i) - (V_5^i - V_7^i) - V_{16}^i\right] \quad (5)$$

$$J_y = (V_6^s - V_{10}^s) - (V_2^s - V_9^s) - V_{17}^s = -\left[(V_6^i - V_{10}^i) - (V_2^i - V_9^i) - V_{17}^i\right] \quad (6)$$

$$J_z = (V_1^s - V_{12}^s) - (V_3^s - V_{11}^s) - V_{18}^s = -\left[(V_1^i - V_{12}^i) - (V_3^i - V_{11}^i) - V_{18}^i\right] \quad (7)$$

$$W_x = (V_1^s + V_{12}^s) - (V_2^s + V_9^s) = -\left[(V_1^i + V_{12}^i) - (V_2^i + V_9^i)\right] \quad (8)$$

$$W_y = (V_3^s + V_{11}^s) - (V_4^s + V_8^s) = -\left[(V_3^i + V_{11}^i) - (V_4^i + V_8^i)\right] \quad (9)$$

$$W_z = (V_5^s + V_7^s) - (V_6^s + V_{10}^s) = -\left[(V_5^i + V_7^i) - (V_6^i + V_{10}^i)\right] \quad (10)$$

$$K_x = (V_4^s - V_8^s) + (V_5^s - V_7^s) = (V_4^i - V_8^i) + (V_5^i - V_7^i) \quad (11)$$

$$K_y = (V_6^s - V_{10}^s) + (V_2^s - V_9^s) = (V_6^i - V_{10}^i) + (V_2^i - V_9^i) \quad (12)$$

$$K_z = (V_1^s - V_{12}^s) + (V_3^s - V_{11}^s) = (V_1^i - V_{12}^i) + (V_3^i - V_{11}^i). \quad (13)$$

Using these relations, it is straightforward to show that the impulses scattered into the stubs can be readily calculated from the quantities U_x, U_y, U_z, J_x, J_y, and J_z:

$$Y_x V_{13}^s = \frac{2Y_x}{4+Y_x} U_x - Y_x V_{13}^i \quad (14)$$

$$Y_y V_{14}^s = \frac{2Y_y}{4+Y_y} U_y - Y_y V_{14}^i \quad (15)$$

$$Y_z V_{15}^s = \frac{2Y_z}{4+Y_z} U_z - Y_z V_{15}^i \quad (16)$$

$$-V_{16}^s = \frac{2Z_x}{4+Z_x} J_x - V_{16}^i \quad (17)$$

$$-V_{17}^s = \frac{2Z_y}{4+Z_y} J_y - V_{17}^i \quad (18)$$

$$-V_{18}^s = \frac{2Z_z}{4+Z_z} J_z - V_{18}^i. \quad (19)$$

In (17) to (19), we use the negative values of the scattered impulses because stubs 16, 17, and 18 are short-circuit. These equations, therefore, include the negative reflections of the stubs. It should be noted that expression (14)–(19) bear exactly the same form.

It is not difficult to establish the physical signification of the quantities U_x, U_y, U_z, J_x, J_y, and J_z. In the original derivation, Johns [5] indicated that they were directly proportional to the magnitudes of the six field components:

$$E_x = 2U_x / u(4+Y_x) \quad (20)$$

$$E_y = 2U_y / v(4+Y_y) \quad (21)$$

$$E_z = 2U_z / w(4+Y_z) \quad (22)$$

$$H_x = -2J_x / Z_0 u(4+Z_x) \quad (23)$$

$$H_y = -2J_y / Z_0 v(4+Z_y) \quad (24)$$

$$H_z = -2J_z / Z_0 w(4+Z_z) \quad (25)$$

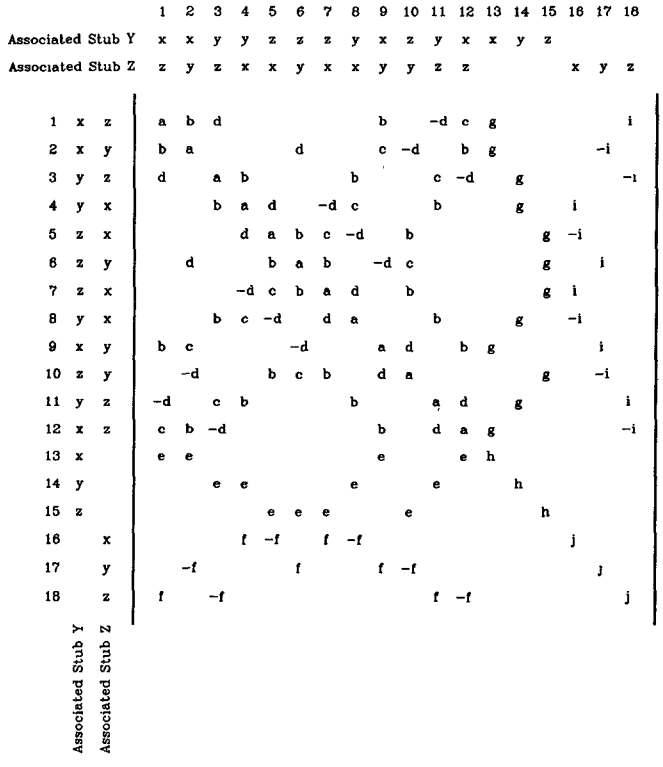

			1	2	3	4	5	6	7	8	9	10	11	12	13	14	15	16	17	18
Associated Stub Y			x	x	y	y	z	z	z	y	x	z	y	x	x	y	z			
Associated Stub Z			z	y	z	x	x	y	x	x	y	y	z	z				x	y	z
1	x	z	a	b	d						b		−d	c	g					i
2	x	y	b	a			d			c	−d		b	g					−i	
3	y	z	d		a	b			b			c	−d		g					−i
4	y	x			b	a	d		−d	c			b		g		i			
5	z	x				d	a	b	c	−d		b				g	−i			
6	z	y		d			b	a	b		−d	c				g		i		
7	z	x				−d	c	b	a	d		b				g	i			
8	y	x			b	c	−d		d	a			b		g		−i			
9	x	y	b	c				−d			a	d		b	g				i	
10	z	y		−d			b	c	b		d	a				g			−i	
11	y	z	−d		c	b				b			a	d		g				i
12	x	z	c	b	−d						b		d	a	g					−i
13	x		e	e							e			e	h					
14	y				e	e				e			e			h				
15	z						e	e	e			e					h			
16		x				f	−f		f	−f								j		
17		y		−f				f			f	−f							j	
18		z	f		−f								f	−f						j

Fig. 2. The characteristics scattering matrix of the symmetrical condensed TLM node.

where u, v, and w are the physical dimensions of the node, and Z_0 is the free-space impedance.

Johns explained that by virtue of conservation of current, the sum of certain current pulses should be the same before and after scattering. This is the physical interpretation of expressions (2)–(7). A comparison between these relations and (20)–(25) reveals that they also express the conservation of field required by Maxwell's equations. The negative sign in expressions (5), (6), and (7) reflects the reversal in direction of current flow after scattering. In the light of this, we can say not only that the symmetrical condensed node satisfies explicitly the law of conservation of energy, S having been derived by Johns from the unitary condition $S^T \cdot S = I$; in addition, electromagnetic fields are also conserved. The symmetrical condensed node requires more numerical effort than the FDTD method because the latter only ensures continuity of fields, and this is only true in the infinitesimal limit, where the node dimensions tend to zero. The symmetrical condensed node, on the other hand, satisfies the field continuity condition even for arbitrary mesh size $u \times v \times w$. Therefore, one should expect the symmetrical condensed node to have better dispersion characteristics than to other networks.

IV. The Algorithm

Now we proceed to show that (2)–(19) can be used to develop an efficient algorithm for TLM analysis. Given the values of the 18 input impulses, we first compute the values of U_r, J_r, W_r, and K_r $(r = x, y, z)$ using (2)–(13). Next the impulses scattered into the stubs can be computed using (14)–(19). Finally, the other scattered impulses can be derived from relations (2)–(13). For example,

$$V_1^s = \{[(U_x - Y_x V_{13}^s) + W_x] + [K_z + (J_z + V_{18}^s)]\}/4 \quad (26)$$

$$V_{12}^s = \{[(U_x - Y_x V_{13}^s) + W_x] - [K_z + (J_z + V_{18}^s)]\}/4 \quad (27)$$

$$V_2^s = \{[(U_x - Y_x V_{13}^s) - W_z] + [K_y - (J_y + V_{17}^s)]\}/4 \quad (28)$$

$$V_9^s = \{[(U_x - Y_x V_{13}^s) - W_x] - [K_y - (J_y + V_{17}^s)]\}/4 \quad (29)$$

Some remarks can be made concerning this procedure:

- For the permittivity stubs, all the expressions involve the current impulse on the stubs only. Thus, it is more convenient to store $Y_x V_{13}$, $Y_y V_{14}$, and $Y_z V_{15}$ than the corresponding voltage impulses V_{13}, V_{14}, and V_{15}.
- The only multiplications appear in (14)–(19). Hence, we need only store six multiplying coefficients for each type of node in order to implement the scattering.
- Equations (2)–(13) contain essentially the sum and difference of the impulses. A sum of any two terms is accompanied by their difference in another expression. This means that a full pipeline program can efficiently handle the manipulations. Parallel processing of the impulses is also advantageous.

By exploiting such features, it is possible to reduce the number of floating point operations to six multiplications, 66 additions/subtractions, and 12 divisions by 4. This count is still considerably higher than the FDTD procedure but is comparable to other expanded nodes. It should be noted that the original scattering matrix requires 144 multiplications and 126 additions/subtractions for direct implementation.

V. Node with Loss

Recently, the symmetrical condensed node has been extended to cover the case of a lossy medium [9]. It was suggested that infinite stubs should be included to simulate energy losses. For lossy dielectric, one extra stub per electric field component is necessary. The total number of ports is therefore 21.

The equations developed above also apply to the lossy node except for certain modifications:

$$U_x = (V_1^s + V_{12}^s) + (V_2^s + V_9^s) + Y_x V_{13}^s + G_x V_{19}^s$$
$$= (V_1^t + V_{12}^t) + (V_2^t + V_9^t) + Y_x V_{13}^t \quad (30)$$

$$U_y = (V_3^s + V_{11}^s) + (V_4^s + V_8^s) + Y_y V_{14}^s + G_y V_{20}^s$$
$$= (V_3^t + V_{11}^t) + (V_4^t + V_8^t) + Y_y V_{14}^t \quad (31)$$

$$U_z = (V_5^s + V_7^s) + (V_6^s + V_{10}^s) + Y_z V_{15}^s + G_z V_{21}^s$$
$$= (V_5^t + V_7^t) + (V_6^t + V_{10}^t) + Y_z V_{15}^t \quad (32)$$

where G_x, G_y, and G_z are the normalized characteristic admittances of the lossy stubs.

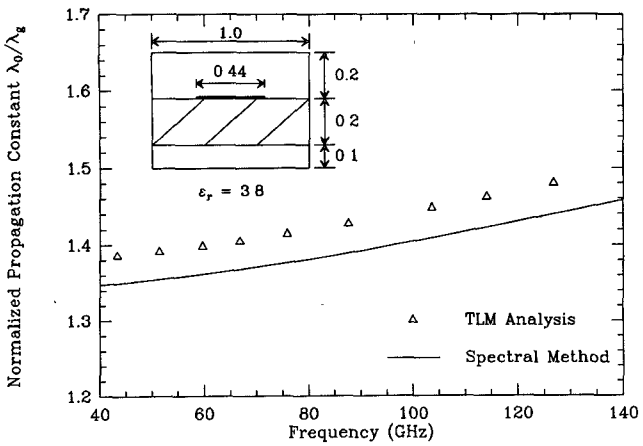

Fig. 3. Dispersion characteristics of a suspended stripline.

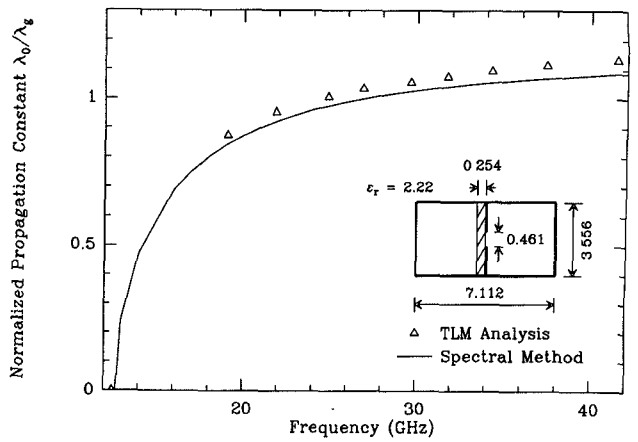

Fig. 4. Dispersion characteristics of a finline.

The supplementary ports offer no input impulses. The impulses scattered into the electric stubs are

$$Y_x V_{13}^s = \frac{2Y_x}{4+Y_x+G_x} U_x - Y_x V_{13}^i \tag{33}$$

$$Y_y V_{14}^s = \frac{2Y_y}{4+Y_y+G_y} U_y - Y_y V_{14}^i \tag{34}$$

$$Y_z V_{15}^s = \frac{2Y_z}{4+Y_z+G_z} U_z - Y_z V_{15}^i \tag{35}$$

$$G_x V_{19}^s = \frac{2G_x}{4+Y_x+G_x} U_x \tag{36}$$

$$G_y V_{20}^s = \frac{2G_y}{4+Y_y+G_y} U_y \tag{37}$$

$$G_z V_{21}^s = \frac{2G_z}{4+Y_z+G_z} U_z. \tag{38}$$

From the user's point of view, unless it is important to know the absolute magnitude of the losses, it is not necessary to store the lost impulses—V_{19}, V_{20}, and V_{21}. That is to say, the basic memory requirement of the lossy node is the same as the original node. By properly manipulating expressions (33)–(38), it is found that the introduction of losses adds only six more multiplications to our algorithm.

VI. Numerical Application

Our algorithm has been implemented in both Fortran and Assembler language. The pipeline features of low-level programming form an excellent environment for the TLM routine. As a consequence, the program written in Fortran running on a Titan super minicomputer is only about three times as fast as that of the Assembler program running on a Compaq 386/25 PC (25 MHz clock). Using single precision, the PC version of the program runs at a speed of 190 μs/node/iteration.

We have successfully applied our algorithm to solve a wide range of electromagnetic problems [10], [11], among them dispersion characteristics, the determination of S parameters, and radiation problems. In order to illustrate the validity of this algorithm, we present here the computed dispersion characteristics of a suspended stripline (Fig. 3) and that of a finline (Fig. 4). The results are compared with those obtained from a standard spectral-domain approach. The precision obtained ranges from 2% to 5%. The values of (λ_0/λ_g) show a higher deviation for the finline because it contains a fine structure of wave diffraction—thin substrate and narrow slot.

VII. Conclusion

We have presented a study of the symmetrical condensed TLM node. The study reveals not only that the characteristics scattering matrix satisfies the law of conservation of energy but also that electromagnetic fields are conserved even for finite node spacing. Using the results of this study, we have been able to develop an efficient algorithm for TLM analysis using the symmetrical condensed node. This algorithm significantly reduces the number of floating point operations so that the speed of computation is comparable to that of other expanded node analysis schemes. The case of lossy medium has also been discussed. Having a better understanding of this symmetrical node and being equipped with a fast algorithm, we believe that TLM analysis of three-dimensional electromagnetic problems can revolutionize the art of computer-aided design of microwave and millimeter-wave circuits.

References

[1] P. B. Johns and R. L. Beurle, "Numerical solution of 2-dimensional scattering problems using a transmission-line matrix," *Proc. Inst. Elec. Eng.*, vol. 118, no. 9, pp. 1203–1208, 1971.

[2] W. J. R. Hoefer, "The transmission-line matrix method—Theory and applications," *IEEE Trans. Microwave Theory Tech.*, vol. MTT-33, pp. 882–893, Oct. 1985.

[3] P. P. M. So, Eswarappa, and W. J. R. Hoefer, "A two-dimensional transmission line matrix microwave simulator using new concepts and procedures," *IEEE Trans. Microwave Theory Tech.*, vol. 37, pp. 1877–1883, Dec. 1989.

[4] R. Allen, A. Mallik, and P. Johns, "Numerical results for the symmetrical condensed TLM node," *IEEE Trans. Microwave Theory Tech.*, vol. MTT-35, pp. 378–382, Apr. 1987.

[5] P. B. Johns, "A symmetrical condensed node for the TLM method," *IEEE Trans. Microwave Theory Tech.*, vol. MTT-35, pp. 370–377, Apr. 1987.

[6] D. A. Al-Mukhtar and J. E. Sitch, "Transmission-line matrix method with irregularly graded space," *Proc. Inst. Elec. Eng.*, vol. 128, pt. H, no. 6, pp. 299–305, 1981.

[7] K. S. Yee, "Numerical solution of initial boundary problems involving Maxwell's equations is isotropic media," *IEEE Trans. Antennas Propagat.*, vol. AP-14, no. 3, pp. 302–307, 1966.

[8] N. Yoshida and I. Fukai, "Transient analysis of a stripline having a corner in three-dimensional space," *IEEE Trans. Microwave Theory Tech.*, vol. MTT-32, pp. 491–498, May 1984.

[9] P. Naylor and R. A. Desai, "New three dimensional symmetrical condensed lossy node for solution of electromagnetic wave problems by TLM," *Electron. Lett.*, vol. 26, no. 7, pp. 492–494, 1990.
[10] C. E. Tong, "Développement d'un récepteur millimétrique à base d'une structure diélectrique incorporant une jonction supraconductrice," thesis accepted by Université de Joseph Fourier, Grenoble, France, Oct. 1988.
[11] C. E. Tong, and Y. Fujino, "Transmission line matrix analysis for three-dimensional electromagnetic problems using personal computer," in *3rd Asia-Pacific Microwave Conf. Proc.* (Tokyo), Oct. 1990, pp. 423–425.

Field Distribution in a Circular Waveguide with a Corrugated Dielectric Lining

Tenneti C. Rao and P. McCormack

Abstract—**The problem of wave propagation through a circular cylinder with a periodically interrupted dielectric lining is solved by a boundary value approach by considering the region between the corrugations as a medium with a tensor permittivity. The characteristic equation for the phase constant is derived by matching the field components. Solutions for the phase constant are obtained and the variation of the phase constant with the physical parameters is studied. The variation of the axial and circumferential electric field components in the transverse plane is also studied.**

I. Introduction

In many applications involving large reflector antenna systems, there is a growing need for a feed structure that will combine the advantages of high gain, low spillover loss, reduced side-lobe level, low cross-polarization, and high aperture efficiency. Thus, Kay [1] in the U.S. and Minnet and Thomas [2] in Australia independently developed the concepts of a corrugated horn and a corrugated circular waveguide, respectively. In the former case, Kay came to the conclusion that grooved walls in a conical horn would present the same boundary conditions to all polarizations and hence would create a tapered aperture field distribution in all planes, resulting in a symmetric radiation pattern with equal E- and H-plane beam widths. Minnet and Thomas showed that the focal region fields of a paraboloidal reflector consisted of a superposition of cylindrical hybrid modes, which are the natural propagating modes of a circular waveguide with corrugated walls. It was realized that such walls are anisotropic in the sense that they impose the same boundary conditions on the electric and magnetic fields, which in turn would lead to an axially symmetric radiation pattern. Clarricoats and Saha [3] carried out a detailed analysis of the propagation and radiation characteristics of a corrugated circular waveguide feed. The radiation pattern and cross-polarization of a dielectric-lined circular waveguide feed were determined by Kumar [4]. If the dielectric lining of the circular waveguide is periodically interrupted, it is believed that the cross-polarization will be significantly reduced, and some preliminary calculations were reported by Mahmoud and Aly [5]. In their study, the region between two disks is considered a medium with tensor permittivity. In the present article, we study the boundary value problem of a dielectric-disk loaded circular waveguide and investigate the propagation characteristics, for example, the phase constant and its variation with the physical parameters of the structure. More details are given elsewhere [6]. Furthermore, the field distribution in the transverse plane is studied; in particular, the variation of the axial and circumferential electric field components with the normalized radius is examined.

Manuscript received July 5, 1990; revised April 24, 1991.

T. C. Rao is with the Electrical Engineering Department, University of Lowell, Lowell, MA 01854.
P. McCormack was with the Electrical Engineering Department, University of Lowell, Lowell, MA. He is now with the Electrical Engineering Department, Tufts University, Medford, MA 02155.

IEEE Log Number 9101370.

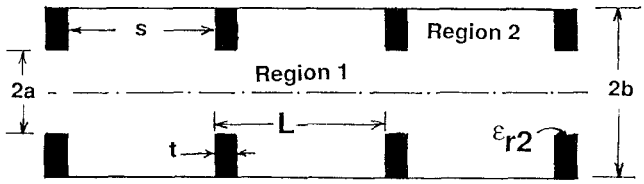

Fig. 1. Geometry of the problem.

II. Solution of the Boundary Value Problem

The geometry of the structure under investigation is shown in Fig. 1. A circular waveguide with an internal diameter of $2b$ exists with its axis coinciding with the z axis of the cylindrical coordinate system (ρ, ϕ, z). The walls of the waveguide are assumed to be perfectly conducting and the waveguide is periodically loaded with dielectric disk of internal diameter $2a$ and external diameter $2b$. The disks have a thickness t and the interdisk spacing is assumed to be s. The relative dielectric constant of the disks is ϵ_{r2} and for generality we assume the region $0 \leqslant \rho \leqslant a$ to have a dielectric constant ϵ_{r1}. The region between $\rho = a$ and $\rho = b$ is assumed to have a tensor permittivity whose components are given by [5]

$$\epsilon = \begin{bmatrix} \epsilon_t & 0 & 0 \\ 0 & \epsilon_t & 0 \\ 0 & 0 & \epsilon_z \end{bmatrix} \tag{1a}$$

where

$$\epsilon_z = \epsilon_0 \epsilon_{r2} / [\epsilon_{r2} - (t/L)(\epsilon_{r2} - 1)] \tag{1b}$$

and

$$\epsilon_t = \epsilon_0 [1 + (\epsilon_{r2} - 1)(t/L)], \qquad L = t + s. \tag{1c}$$

The axial components of the electric and magnetic fields in region 1 $(0 \leqslant \rho \leqslant a)$ are given by

$$E_{z1} = A_1 J_1(k_1 \rho) \cos\phi \exp(-j\beta z) \tag{2a}$$

$$\eta_0 H_{z1} = B_1 J_1(k_1 \rho) \sin\phi \exp(-j\beta z) \tag{2b}$$

where A_1 and B_1 are the amplitude constants, $J_1(k_1\rho)$ is the Bessel function of the first kind and order 1, and β is the axial phase constant. The transverse wavenumber is given by $k_1 = (k_0^2 \epsilon_{r1} - \beta^2)^{1/2}$, where k_0 is the free-space wavenumber $(\omega\sqrt{\mu_0 \epsilon_0})$. In a similar manner, the axial components of the electric and magnetic fields in region 2 $(a \leqslant \rho \leqslant b)$ can be